

Composite optical vortices

Ivan D. Maleev and Grover A. Swartzlander, Jr.

Optical Sciences Center, University of Arizona, Tucson, Arizona 85721

Received October 7, 2002; revised manuscript received February 19, 2003

Composite optical vortices may form when two or more beams interfere. Using analytical and numerical techniques, we describe the motion of these optical phase singularities as the relative phase or amplitude of two interfering collinear nonconcentric beams is varied. The creation and the annihilation of vortices are found, as well as vortices having translational velocities exceeding the speed of light. © 2003 Optical Society of America

OCIS codes: 350.5030, 260.3160, 260.0260, 030.1670, 030.6140.

1. INTRODUCTION

Optical vortices¹ (OVs) or “phase defects” often occur in coherent radiation, e.g., in Laguerre–Gaussian laser beams,² light scattered from rough surfaces,^{3,4} optical caustics,^{5,6} and OV solitons.^{7,8} The center of the vortex is characterized by a dark core, within which the intensity vanishes at a point, assuming the beam is coherent.^{9,10} The phase front of an OV is helical, and thus the wave vectors have azimuthal components that circulate around the core.¹¹ Owing to this circulation, the optical wave carries orbital angular momentum.¹² In general, when one beam is superimposed with another, the phase of the composite field differs from that of the component beams. Being a topological phase structure, an optical vortex is readily affected when it is combined with other fields. The new or “composite vortex” may be repositioned in space or annihilated, and other vortices may spontaneously form in the net field.^{13–15} The velocity at which a vortex actually moves depends on how quickly parameters such as the relative phase or amplitude can be varied. For example, the rate of change of the amplitude can be so large for an ultrashort pulse of light that the vortex speed exceeds that of light. This finding does not violate the principles of relativity because the vortex velocity is a phase velocity.

An interest in OVs traces back to 1974, when Nye and Berry showed that coherent waves reflected from rough surfaces contain phase defects; namely edge, screw, and phase dislocation.^{3,5} Practical interest was sparked by Lukin *et al.*, who considered phase fluctuations of light beams in the atmosphere.¹⁶ In 1981, Baranova *et al.*⁴ showed that laser speckle contains a large number of randomly distributed OVs. In the 1990s, Coulet *et al.*¹⁷ stimulated an interest in nonlinear OVs in laser cavities, while Swartzlander and Law experimentally and numerically discovered the OV soliton in self-defocusing media.⁷ The latter group was also the first to describe the creation of optical vortices by destabilizing dark-soliton stripes.^{7,18} Soskin *et al.*^{13–15} laid groundwork for new experimental methods in linear and nonlinear OV phenomenon. Staliunas,¹⁹ Indebetouw,²⁰ and Freund²¹ established an understanding of vortex propagation. Owing to their particlelike nature, OVs were said to repulse or attract

each other,²² or to split, annihilate, or be born²³ as a complex system of vortices.⁶ The propagation dynamics of optical vortices was clarified by Rozas *et al.*²⁴ The fluid-like rotation of propagating optical vortices around a common center was discussed by Roux²⁵ and observed for the special case of small-core OVs by Rozas *et al.*²⁶ Most recently, the phase of globally linked vortex clusters has been described.²⁷

Thus far, the study of beam combinations has been limited to the coherent coaxial superposition of several beams.¹ For example, Soskin and Vasnetsov showed that a coherent background field changes the position of an OV and can lead to the destruction and creation of vortices. Recent investigations of the presence of incoherent light within the vortex core has been reported.^{9,10}

In this paper, we describe OVs in the superimposed field of two parallel, noncollinear beams. We map the position and topological charge of the OVs as the relative phase or distance between the two beams is varied. For consistency with experimental approaches, we numerically generate interferograms that allow the determination of the position and topological charge of vortices in the composite field.

2. SINGLE OPTICAL VORTEX

An optical vortex (Fig. 1) is essentially a phase object, and thus it is necessary to assume that the beam containing it exhibits transverse coherence (at least in the proximity of the vortex core). A single optical vortex placed at the center of a cylindrically symmetrical coherent beam may be represented by the complex electric field in the transverse (x, y) plane:

$$E(r, \theta) = A \exp(i\beta) \times f(r) \exp(im\theta), \quad (1)$$

where (r, θ) are circular transverse coordinates in the ($x = r \cos \theta, y = r \sin \theta$) plane (we assume the vortex core coincides with the origin, $r = 0$), A is a measure of the field amplitude (assumed to be real), β is an arbitrary phase constant, $f(r)$ is a real function representing the profile of the beam envelope, and m is the topological charge of the vortex (a signed integer). The amplitude and the phase (A and β) may vary with time. Note that

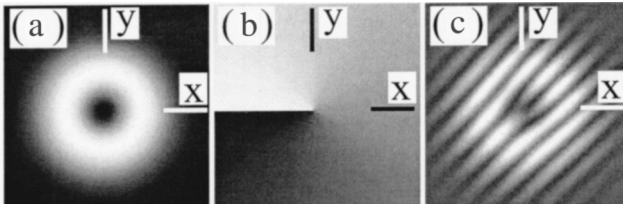


Fig. 1. Single optical vortex of charge $m = 1$ in a Gaussian field. (a) Intensity profile. (b) Phase profile showing a singular point at the origin. (c) Interferogram showing a forking pattern in the vicinity of the vortex.

the phase factor, $\exp(im\theta)$, is undefined at the vortex-core position, $r = 0$ [Fig. 1(b)]. For this reason, a vortex is sometimes called a phase singularity. In three dimensions, the surface of constant phase is a construction of $|m|$ helices having a common axis and a pitch equal to the wavelength, λ . For the special case $m = 0$, the wave front is planar. In principle, any vortex of nonzero topological charge, m , may be treated as the product of $|m|$ vortices, each having a fundamental charge of ± 1 . Thus for simplicity, we consider only beams with fundamental values, $m = -1, 0$, or $+1$. Below, we make use of the relation between the amplitude, A , and power, P , of the beam in Eq. (1):

$$A = \left[P \int_0^\infty r f^2(r) dr \right]^{1/2}. \quad (2)$$

Owing to total destructive interference, a characteristic of an optical vortex is a point of zero intensity in the dark vortex core. Analytically, the position of this zero may be found by considering that both the real and the imaginary parts of the field must vanish:

$$\text{Re}\{E\} = Af(r)\cos(m\theta + \beta) = Ar^{-1}f(r)x' \equiv 0, \quad (3a)$$

$$\text{Im}\{E\} = Af(r)\sin(m\theta + \beta) = Ar^{-1}f(r)y' \equiv 0, \quad (3b)$$

where $(x', y') = (r \cos(m\theta + \beta), r \sin(m\theta + \beta))$ are rotated coordinates. Both Eqs. (3a) and (3b) vanish identically at the origin for any physically meaningful function,

$$g(r) = (w_0/r)f(r), \quad (4)$$

where w_0 is the characteristic beam size. In this paper, we restrict ourselves to Gaussian beam profiles: $g(r) = \exp(-r^2/w_0^2)$.

To detect optical vortices in the laboratory, it is not sufficient to simply identify the points of zero intensity. Instead, one must obtain information about the phase to verify that it is spatially harmonic (when satisfied, this condition also satisfies the requirement that the intensity vanishes at the core). Interferometry allows us to do this while also determining the location and the topological charge. The interferogram of a vortex displays a characteristic forking pattern [Fig. 1(c)]. For example, when the vortex field described by Eq. (1) is interfered with a planar reference wave given by $E' = A' \exp(ik_x x)$, where k_x is the transverse wave number of the tilted plane wave, the interferogram has a profile given by

$$|E + E'|^2 = A^2 f^2 + A'^2 + 2AA' f \cos(m\theta + \beta - k_x x). \quad (5)$$

Far from the center of the vortex, the interferogram displays lines of constant phase that are nearly parallel to the y axis. At the center of the core (the origin), the intensity of the interferogram has a value of A'^2 . Above ($x \approx 0, y > 0$) and below ($x \approx 0, y < 0$) the phase singularity, the value of the factor $\cos(m\theta + \beta - k_x x)$ switches sign, thereby creating a forking pattern. In practice, the approximate locations of vortices are found by locating the vertex of these forks, and the precise position is found by removing the reference wave and determining the position of minimum intensity.

3. COMPOSITE VORTICES

When two or more beams described by Eq. (1) and possibly having different centroids are superimposed, the resultant zero-intensity points in the composite beam do not generally coincide with those of the individual beams. We expect the 'new' composite vortices, being phase objects, to depend on the relative phase and amplitude of the individual beams. Let us first examine the superposition of two mutually coherent beams containing vortices under steady-state conditions. The composite field is given by

$$E(r, \theta) = \sum_{j=1}^2 A_j g(r_j)(r_j/w_0)^{|m_j|} \exp(im_j \theta_j) \exp(i\beta_j), \quad (6)$$

where (r_j, θ_j) are the transverse coordinates measured with respect to the center of the j th beam, and β_j is the phase of the j th beam. In the laboratory, the location of the composite vortices may be found with interferometry, as discussed above, where the intensity profile of the interferogram is given by

$$|E + A' \exp(ik_x x)|^2 = |E|^2 + A'^2 + 2|E|A' \cos(\Phi - k_x x), \quad (7)$$

where $\Phi = \arctan(\text{Im}\{E\}/\text{Re}\{E\})$. As we saw in the previous section, the intensity of the interferogram at the location of a composite vortex has a value given by A'^2 (since $|E| = 0$), and forking patterns are expected around the singular points, where Φ is undefined.

For convenience, we consider two beams displaced along the x axis by a distance $\pm s$ from the origin, as shown in Fig. 2, where beam 1 and beam 2 appear on the right and the left, respectively. The relative displacement compared with the beam size is defined by

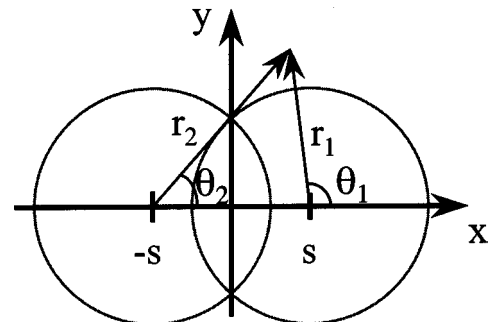


Fig. 2. Two beams of radial size w_0 separated by a distance $2s$. Bipolar coordinates are labeled.

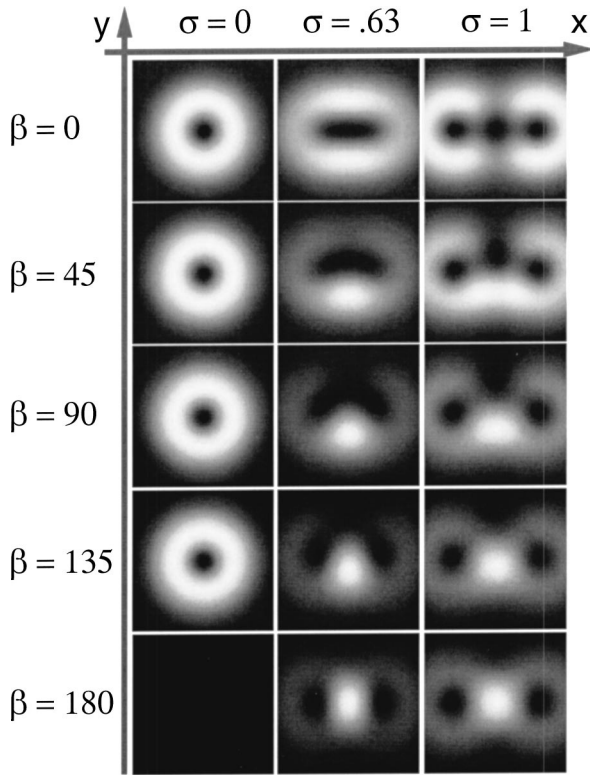


Fig. 3. Phase (β) and separation ($\sigma = s/w_0$) dependent intensity patterns of a composite beam created by superimposing two equal amplitude $m = 1$ vortex beams. Coaxial component beams ($\sigma = 0$) uniformly and destructively interfere. For $\sigma > 0$, one or three vortices form when the phase is below or above a critical value. The third vortex leaves the beam region.

$\sigma = (s/w_0)$. One may readily verify that the bipolar coordinates $(r_1, \theta_1, r_2, \theta_2)$ are related to the circular coordinates (r, θ) by the relations

$$r_1 \exp(\pm i \theta_1) = r \exp(\pm i \theta) - s, \quad (8a)$$

$$r_2 \exp(\pm i \theta_2) = r \exp(\pm i \theta) + s. \quad (8b)$$

Without loss of generality, we define the relative phase, $\beta = \beta_1 - \beta_2$, and set $\beta_2 = 0$. In many cases the symmetry of the phase-dependent vortex motion will allow us to simply consider values of β between 0 and π . Let us now consider three representative cases of combined beams, where the topological charges are identical ($m_1 = m_2$), opposite ($m_1 = -m_2$), and different ($m_1 = 1, m_2 = 0$).

Case 1

If we superimpose two singly charged vortex beams having identical charges, say, $m_1 = m_2 = +1$, then the composite field in Eq. (6) may be expressed

$$E(r, \theta) = [A_1 g_1(r_1) \exp(i\beta) + A_2 g_2(r_2)](r/w_0) \exp(i\theta) - [A_1 g_1(r_1) \exp(i\beta) - A_2 g_2(r_2)](s/w_0). \quad (9)$$

The intensity profiles, $|E|^2$, for various values of phase and separation are shown in Fig. 3. Setting the real and the imaginary parts of Eq. (9) to zero, we find composite vortices located at the points (x, y) that satisfy the transcendental equation

$$x + iy = s \tanh[2\sigma^2 x/s + (1/2)\ln(A_1/A_2) + i\beta/2]. \quad (10)$$

Several special cases of Eq. (10) can be readily identified and solved.

Let us first consider the in-phase and equal-amplitude case: $\beta = 0$ and $A_1 = A_2$, which allows solution only along the x axis (see the top row in Fig. 3). A solution of Eq. (10) exists at the origin for any value of σ ; however, we find its sign changes from positive to negative when σ increases beyond the critical value:

$$\sigma_{cr} = 2^{-1/2}. \quad (11)$$

What is more, for $\sigma > \sigma_{cr}$, two additional $m = 1$ vortices emerge. One may easily verify this critical value by expanding the hyperbolic tangent function in Eq. (10) to third order, assuming $|x/s| \ll 1$, and thereby obtaining

$$|x/s| \cong [3(2\sigma^2 - 1)/8\sigma^6]^{1/2}. \quad (12)$$

For well separated beams, $\sigma \gg \sigma_{cr}$, a first-order expansion of Eq. (10) indicates that the composite vortices are displaced toward each other ($|x/s| < 1$), and, as expected, they nearly coincide with the location of the original vortices:

$$|x/s| \cong 1 - 2 \exp(-4\sigma^2 x/s). \quad (13)$$

Let us next consider the out-of-phase, equal-amplitude case: $\beta = \pi, A_1 = A_2$ (see bottom row in Fig. 3). In this case, we find two vortices for all values of σ , with an additional vortex at $y = \pm\infty$. For the special case $\sigma = 0$, total destructive interference occurs, and the composite field vanishes. Again, we find the solutions are constrained to the x axis, but now the positions are given by

$$x/s = \coth(2\sigma^2 x/s). \quad (14)$$

The vortices are displaced away from each other and their original position ($|x/s| > 1$), and for $\sigma \gg \sigma_{cr}$,

$$|x/s| \cong 1 + 2 \exp(-4\sigma^2 x/s). \quad (15)$$

These analytical results and the numerically calculated intensity profiles in Fig. 3 demonstrate that the vortex core may be readily repositioned by changing the relative position or phase of the component beams. From an experimental and application point of view, the later variation is often easier to achieve in a controlled linear fashion. For example, the net field may be constructed from two collinear beams from a Mach-Zehnder interferometer, whereby the phase is varied by introducing an optical delay in one arm of the interferometer.

A demonstration of the phase-sensitive vortex trajectory is shown in Fig. 4 for the case $\sigma = 0.47$ (i.e., $\sigma < \sigma_{cr}$). We find that a critical value of phase exists such that, for $|\beta| < \beta_{cr}$, there is a single composite vortex of charge $m = 1$, and it resides on the y axis. Above the critical phase, two $m = 1$ vortices split off from the y axis, and, simultaneously, one $m = -1$ vortex remains on the y axis. The value of the topological charge may be found by examining numerically generated phase profiles or interferograms of Eq. (9). The positively charged vortices (see the black dots in Fig. 4) circumscribe the position of the original vortices (indicated by isolated gray dots in Fig. 4).

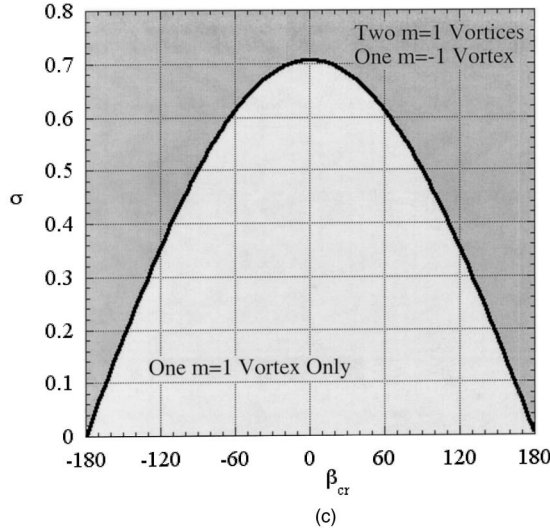
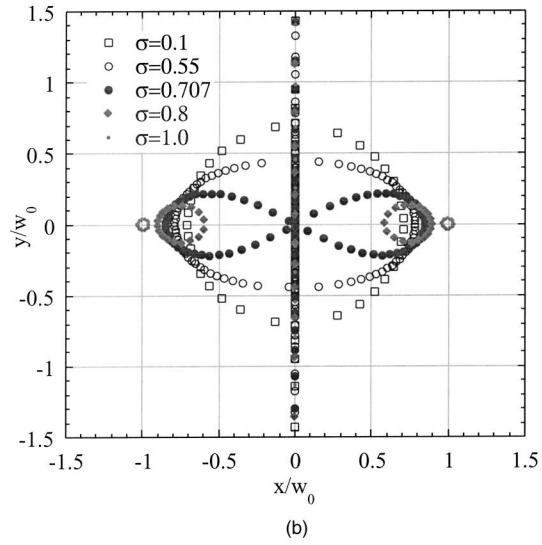
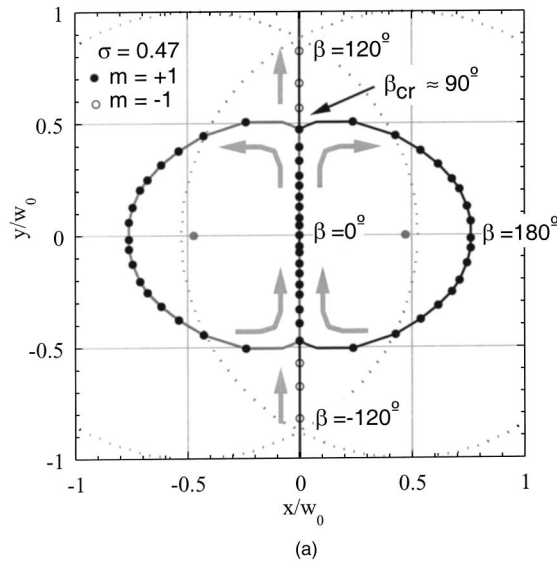


Fig. 4. Phase-dependent composite vortex trajectories resulting from the superposition of two equal-amplitude $m = 1$ component beams. (a) $\sigma = 0.47$ showing a single $m = 1$ vortex for $\beta < \beta_{cr}$, and two $m = 1$ and one $m = -1$ for $\beta > \beta_{cr}$. Arrows indicate the direction of motion for increasing values of β . Dotted curves demarcate the footprints of the component beam waists. (b) Family of trajectories for different values of σ . (c) A third vortex appears in all cases when β exceeds a separation-dependent critical value. For $\sigma > \sigma_{cr} = 2^{-1/2}$, three vortices always exist, and the trajectory of the two $m = 1$ vortices become separate closed paths.

The net topological charge is $m_{net} = 1$ for all values of β , and, being unequal to the sum of charges of the original beams ($m_{sum} = 2$), is therefore not conserved in the sense that $m_{net} \neq m_{sum}$. From a practical point of view, however, we note that the $m = -1$ vortex escapes toward $|y| = \infty$ when $\beta \approx \pi$. Furthermore, the field amplitude surrounding the escaping vortex is negligible and is therefore unobservable. Empirically, this leads one to the observation that the net topological charge is sometimes conserved in a “weak sense.”

Phase-dependent vortex trajectories for different values of the separation parameter, σ , are shown in Fig. 4(b). For $\sigma < \sigma_{cr}$, a single $m = 1$ vortex resides on the y axis when $|\beta| < \beta_{cr}$; above the critical phase, an $m = -1$ vortex continues moving on the y axis toward infinity, while two $m = 1$ vortices form symmetric paths that circumscribe the positions of the original vortices. For $\sigma > \sigma_{cr}$, three vortices always exist, with one having charge $m = -1$ constrained to the y axis and the other two having charge $m = 1$ circling the original vortices. As discussed above for Fig. 4(a), the net topological charge is never strictly conserved for the cases in Fig. 4(b).

The value of β_{cr} may be estimated from Eq. (10) by expanding the hyperbolic tangent function in the vicinity of $x/w_0 = 0$. To first order, we find

$$2\sigma^2[1 + \tan^2(\beta_{cr}/2)] \approx 1. \tag{16}$$

For $\sigma = 0.50$, we obtain $\beta_{cr} \cong 90^\circ$, in good agreement with the numerically obtained value.

A qualitative understanding of the composite vortex generation can be formed by examining Fig. 3. When $\sigma = 0$, we have the simple interference between beams having different phases. When $\sigma = 0.63$, we find an elongated composite beam having a single vortex when $\beta = 0$, but the emergence of two $m = 1$ and one $m = -1$ vortices when $\beta_{cr} < \beta < \pi$.

Case 2

For two oppositely charged vortices ($m_1 = -m_2 = +1$), Eq. (6) becomes

$$\begin{aligned}
E(r, \theta) = & [A_1 g_1(r_1) \exp(i\beta) \exp(i\theta) \\
& + A_2 g_2(r_2) \exp(-i\theta)] (r/w_0) \\
& - [A_1 g_1(r_1) \exp(i\beta) - A_2 g_2(r_2)] (s/w_0).
\end{aligned} \tag{17}$$

The intensity profiles for different values of phase and separation, shown in Fig. 5, are qualitatively different than those for case 1 (see Fig. 3). To determine the position of vortices, we set Eq. (17) to zero. It happens that the zero-valued field points for both the in-phase and out-of-phase cases, $\beta = 0$ and $\beta = \pi$, must satisfy the equations

$$x = s \tanh[2\sigma^2 x/s + (1/2)\ln(A_1/A_2) + i\beta/2], \tag{18a}$$

$$y \sinh[2\sigma^2 x/s + (1/2)\ln(A_1/A_2) + i\beta/2] = 0. \tag{18b}$$

For the in-phase equal-amplitude case ($\beta = 0, A_1 = A_2$), there are zeros that do not correspond to a vortex but rather to an edge dislocation (i.e., a division between two regions having a phase difference of π). The first row in Fig. 5 shows, for different values of σ , the dislocation as a black line bisecting two halves of the composite beam. Vortices do not appear in this in-phase case unless $\sigma > \sigma_{cr}$ [see Eq. (11)], whence they occur on the x axis and are described by the same limiting relations as we found in case 1 [i.e., Eqs. (12) and (13)]. The out-of-phase equal amplitude ($\beta = \pi, A_1 = A_2$) solutions are also identical to those found in case 1 [see Eq. (14)].

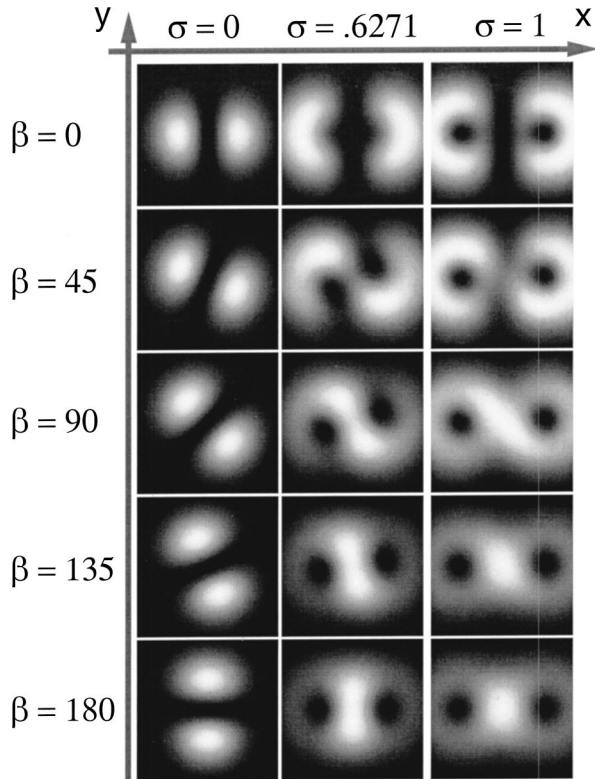


Fig. 5. Same as Fig. 3 except $m_1 = 1$ and $m_2 = -1$. Coaxial component beams ($\sigma = 0$) form an edge dislocation, dividing the composite beam. This dislocation persists for all values of σ when $\beta = 0$. Composite vortices appear as an oppositely charged pair (dipole).

The composite vortex positions in case 2 are generally different than case 1 for arbitrary values of β and σ . For example, in case 1 we found either one or three vortices, while in case 2 there are always two vortices. Whereas the vortex positions in case 1 appeared symmetrically across the y axis for $|\beta| > |\beta_{cr}|$, they appear at radially symmetric positions in case 2 for all values of β . Finally, we note that, when $\sigma = 0$ in case 2, the two original vortices interfere for all values of β to produce an edge dislocation, as shown in the left-hand column of Fig. 5, whereas in case 1 the beams uniformly undergo progressive destructive interference.

The phase-dependent vortex trajectory for $\sigma = 0.47$ is shown in Fig. 6(a). Indeed, it differs from the trajectory for case 1 shown in Fig. 4(a). At $\beta = \epsilon$ (where $\epsilon \ll 1$), we find in Fig. 6(a) an $m = 1$ vortex at a point on the positive y axis and an $m = -1$ vortex at the symmetrical point on the negative y axis. As the phase advances, the vortex positions rotate clockwise. Curiously, we find that, as the phase is varied slightly from $\beta = -\epsilon$ to $\beta = +\epsilon$, the vortices suddenly switch signs. This switch may also be interpreted as an exchange of the vortex positions. In either case, this exchange occurs via an edge dislocation at the phase $\beta = 0$. Edge dislocations are often associated with sources or sinks of vortices.^{7,18,28,29} Unlike case 1, we find that the net topological charge is conserved for all values of β , i.e., $m_{net} = m_{sum}$.

Generic shapes of the composite vortex phase-dependent trajectories are shown in Fig. 6(b) for different separation distances. For small values of separation ($\sigma \ll 1$), the path of each vortex is nearly semicircular, with vortices on opposing sides of the origin. When $\sigma \geq \sigma_{cr}$, each vortex trajectory forms a separate closed path. Regardless of the value of s , the vortex on the right has a charge, $m = 1$, opposite of that of the left. As found in case 1, the critical separation distance delineates open-path and closed-path trajectories. The topological charge is conserved for all the values of β and σ in Fig. 6, and thus, by induction, we conclude that the net topological charge is always conserved for case 2.

Case 3

Last, we consider the interference between beams having a vortex (beam 1) and planar (beam 2) phase: $m_1 = 1, m_2 = 0$. Examples of the intensity profiles are shown in Fig. 7. Substitution of the values of m into Eq. (6) gives

$$\begin{aligned}
E(r, \theta) = & A_1 g_1(r_1) \exp(i\beta) (r/w_0) \exp(i\theta) + A_2 g_2(r_2) \\
& - A_1 g_1(r_1) \exp(i\beta) (s/w_0).
\end{aligned} \tag{19}$$

Zero field points must satisfy

$$(x + iy)/s = 1 - \sigma^{-1} (A_2/A_1) \exp(-i\beta) \exp(-4\sigma^2 x/s). \tag{20}$$

Let us consider the case when the vortex and Gaussian beams have the same power. From Eq. (2), we obtain the relation between the amplitudes of the vortex, A_1 , and Gaussian, A_2 , beams:

$$A_1 = 2^{1/2} A_2. \tag{21}$$

In the in-phase case ($\beta = 0$), Eq. (20) simplifies to

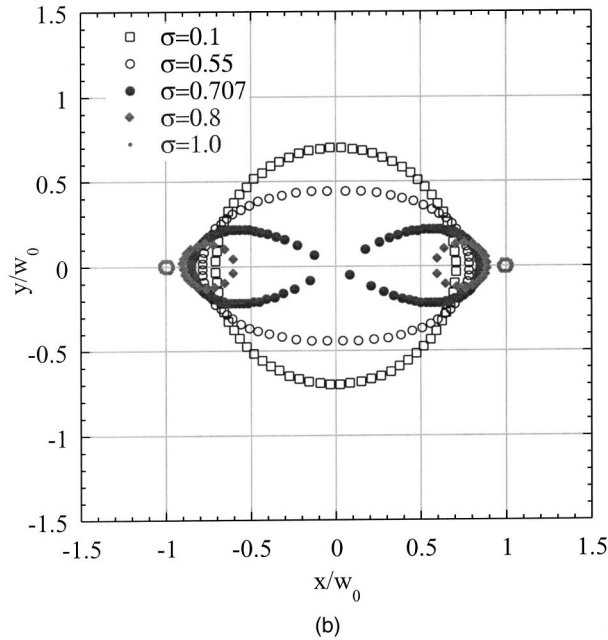
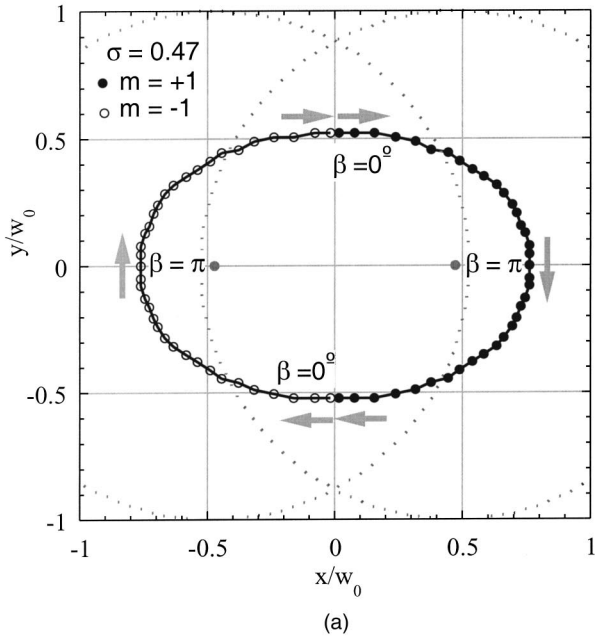


Fig. 6. Phase-dependent composite vortex trajectories for $m_1 = 1$ and $m_2 = -1$. (a) $\sigma = 0.47$, showing a rotating composite vortex dipole whose orientation flips when $\beta = 0_+$ and $\beta = 0_-$. Arrows indicate the direction of motion for increasing values of β . Dotted curves demark the footprints of the component beam waists. (b) Family of trajectories for different values of σ . For $\sigma > \sigma_{cr} = 2^{-1/2}$, the trajectories become separate closed paths.

$$(x + iy)/s = 1 - \sigma^{-1} 2^{-1/2} \exp(-4\sigma^2 x/s), \quad (22)$$

which has solutions only along the x axis, and two critical points $\sigma_1 \approx 0.1408$ and $\sigma_2 \approx 0.6271$, which are the solutions of the transcendental equation

$$2^{3/2} \sigma = \exp(4\sigma^2 - 1). \quad (23)$$

The in-phase case has no solutions if $\sigma_1 < \sigma < \sigma_2$ (although a dark spot may form in the composite beam), one

solution if $\sigma = \sigma_1$ ($x/s \approx -11.6$) or $\sigma = \sigma_2$ ($x/s \approx 0.364$), and two solutions otherwise.

Two other cases of special interest exist. An exact solution of Eq. (20) is found for any value of σ when $\beta = \pi/2$:

$$x = s, \quad (24a)$$

$$y = (w_0/2^{1/2}) \exp(-4s^2/w_0^2). \quad (24b)$$

For the out-of-phase case, $\beta = \pi$, Eq. (20) simplifies to

$$(x + iy)/s = 1 + \sigma^{-1} 2^{-1/2} \exp(-4\sigma^2 x/s), \quad (25)$$

which allows a single composite vortex solution on the x axis, whose position is displaced away from the Gaussian ($m = 0$) beam.

Numerically determined vortex positions are shown in Fig. 8(a) for $\sigma = 0.47$. Since this value falls between the two critical values, there are no composite vortices for the in-phase case. In fact, we find no vortices over the range $|\beta| < \beta_{cr}$. The critical phase value depends on the value of σ , and in this case $\beta_{cr} \approx 40^\circ$. In general, the critical phase may be computed from the relation $(2^{3/2} \sigma \cos \beta_{cr}) \exp(4\sigma^2 - 1) = 1$. The gray curve with diamonds in Fig. 8(a) indicates the position of a dark (but nonzero) intensity minimum that appears when $|\beta| < \beta_{cr}$. Owing to their darkness, these points could be mistaken for vortices in the laboratory if interferometric measurements are not recorded to determine the phase. Beyond the critical phase value, we find an oppositely

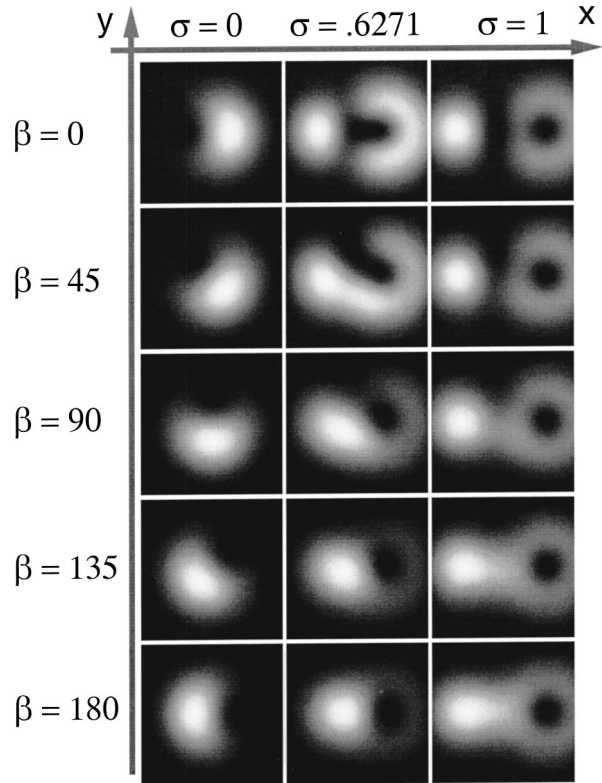


Fig. 7. Phase (β) and separation (σ) dependent intensity patterns of a composite beam created by superimposing vortex ($m_1 = 1$) and nonvortex ($m_2 = 0$) component beams. Both beams have equal power. The composite beam contains either no vortices or a vortex dipole with the $m = -1$ vortex often residing far from the beam region.

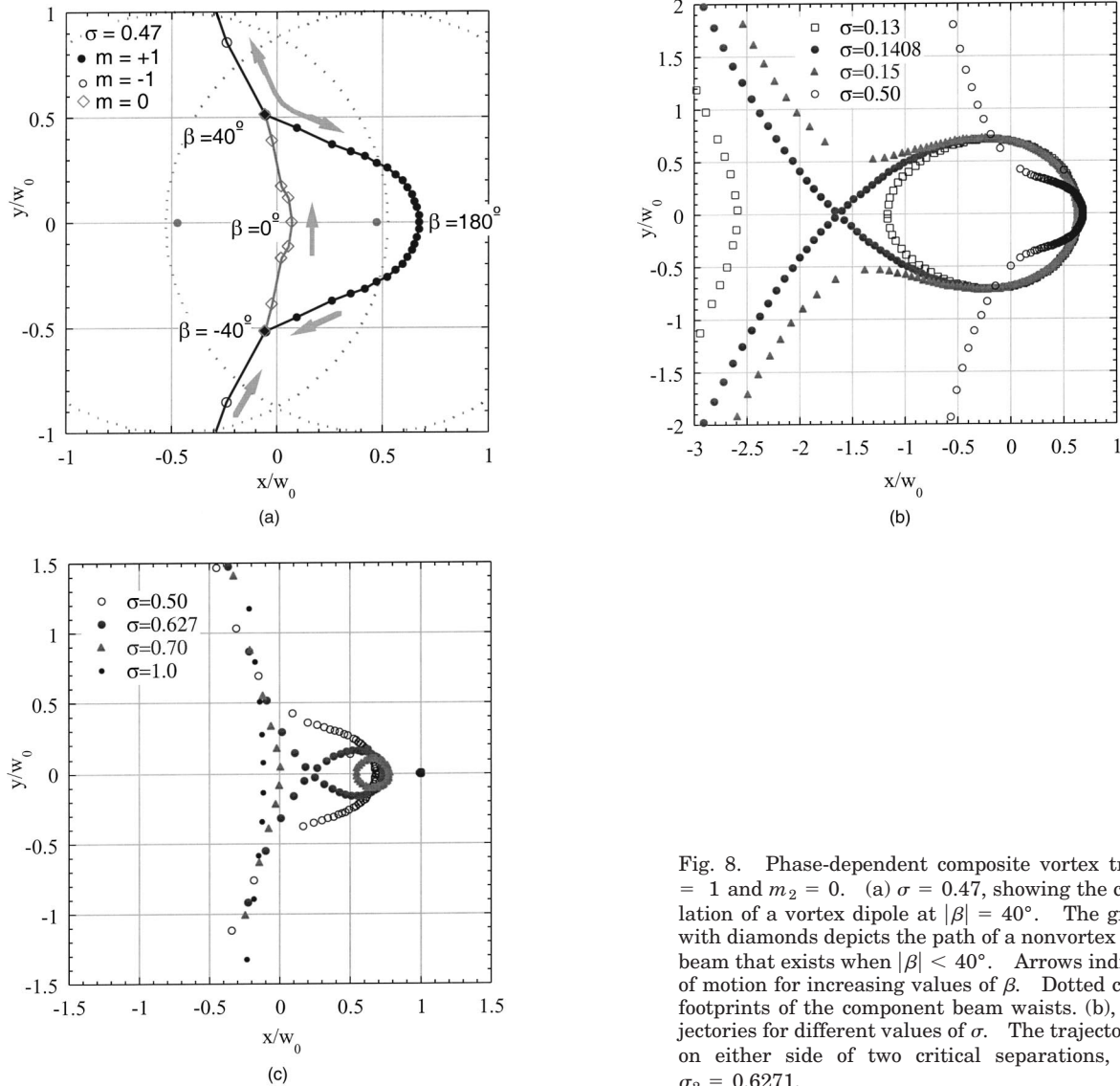


Fig. 8. Phase-dependent composite vortex trajectories for $m_1 = 1$ and $m_2 = 0$. (a) $\sigma = 0.47$, showing the creation or annihilation of a vortex dipole at $|\beta| = 40^\circ$. The gray curve marked with diamonds depicts the path of a nonvortex dark region of the beam that exists when $|\beta| < 40^\circ$. Arrows indicate the direction of motion for increasing values of β . Dotted curves demarcate the footprints of the component beam waists. (b), (c) Family of trajectories for different values of σ . The trajectories change shape on either side of two critical separations, $\sigma_1 = 0.1408$ and $\sigma_2 = 0.6271$.

charged pair of vortices, with the positively charged vortex remaining in close proximity to the $m = 1$ vortex of beam 1 and the negatively charged vortex diverging from the region as the phase increases. Regardless of the value of β , we find the net topological charge, $m_{\text{net}} = 0$, is not equal to the sum, $m_{\text{sum}} = 1$.

Figures 8(b) and 8(c) depict vortex trajectories as the phase is varied for a number of different values of σ . The trajectories for σ_1 and σ_2 resemble strophoids, separating regions having open and closed paths. For example, if $\sigma_1 < \sigma < \sigma_2$, a vortex dipole is created or annihilated at a point at some critical phase value; thus the trajectory of each vortex is an open path. On the other hand, for $\sigma < \sigma_1$ or $\sigma > \sigma_2$, the dipole exists for all values of β , and the paths are closed. The rightmost vortex in all these cases has a charge $m = 1$.

Inspections of phase profiles indicate that the net topological charge is $m_{\text{net}} = 0$ for all values of σ and β shown in Fig. 8, except for the degenerate case,¹ $\sigma = 0$ (see left-hand column in Fig. 7), where $m_{\text{net}} = 1$. The case $\sigma = 0.13$, shown in Fig. 8(b), suggests that, when the relative separation is small ($\sigma \ll 1$), one vortex having the

same charge as beam 1 circles the origin, while a second vortex of the opposite charge appears in the region beyond the effective perimeter of the beam. As a practical matter, one may ignore the existence of the second vortex if it is surrounded by darkness, and in this case, one may state that the charge is conserved in a weak sense. However, the second vortex is not always shrouded in darkness. Thus the superposition of a vortex and a Gaussian beam does not generally conserve the net value of the topological charge.

4. VORTEX VELOCITY

The superposition of a vortex and Gaussian beam provides a particularly convenient means of displacing a vortex, owing to the common availability of Gaussian beams from lasers. By rapidly changing the amplitude of the Gaussian beam, the vortex may be displaced at rates that exceed the speed of light without moving the beams or varying the phase. The speed of the vortex may be determined by applying the chain rule,

$$v_x + iv_y = \left(\frac{\partial x}{\partial A_2} + i \frac{\partial y}{\partial A_2} \right) \frac{dA_2}{dt}, \quad (26)$$

where $(x + iy)$ is given by the transcendental function, Eq. (20). The solution for the velocity simplifies when $\beta = \pi/2$, in which case $x = s$, $v_x = 0$, and $v_y = (s/\sigma A_1) \exp(-4\sigma^2) dA_2/dt$. The vortex traverses the beam at a speed that exceeds the speed of light when $dA_2/dt > (A_2/\tau_0) \exp(4\sigma^2)$, where $\tau_0 = w_0/c$ is the time it takes light to travel the distance w_0 . A relatively slow light pulse may be used to achieve this if w_0 is large and $\sigma = 0$ (note that any value of β may be used when $\sigma = 0$). Assuming the amplitude of the Gaussian beam increases linearly with a characteristic amplitude, \hat{A}_2 , and time τ_2 , $A_2(t) = (\hat{A}_2/\tau_2)t$, then light speed may be achieved when $\hat{A}_2/A_1 > \tau_2/\tau_0$. This may be satisfied with a beam having a 100-ps rise time and a 30-mm radial beam size, assuming $\hat{A}_2/A_1 = 1$.

5. CONCLUSION

Our investigation of the superposition of two coherent beams, with at least one containing an optical vortex, reveals that the transverse position of the resulting composite vortex can be controlled by varying a control parameter such as the relative phase, amplitude, or distance between the composing beams. The three most fundamental combinations of beams were explored, namely, beams having identical charges, beams having opposite charges, and the combination of a vortex and Gaussian beam. Composite vortices were found to rotate around each other, merge, annihilate, or move to infinity. We found that the number of composite vortices and their net charge did not always correspond to the respective values for the composing beams. As may be expected from the principle of conservation of topological charge, the net composite charge remained constant as we varied the control parameters. Critical conditions for the creation or annihilation of composite vortices were determined. Composite vortex trajectories were found for special cases. The superposition of oppositely charged vortex beams produced composite vortices that remained in the beam, whereas other cases had vortices that diverged toward infinity. The speed of motion along a trajectory was demonstrated to depend on the rate of change of the control parameter. For example, we described how the speed of a vortex may exceed the speed of light by rapidly varying the amplitude of one of the beams.

ACKNOWLEDGMENT

This work was supported by funds from the State of Arizona.

REFERENCES

- M. V. Vasnetsov and K. Staliunas, eds., *Optical Vortices*, Vol. 228 in *Horizons in World Physics* (Nova Science, Huntington, N.Y., 1999).
- A. E. Siegman, *Lasers* (University Science, Mill Valley, Calif., 1986).
- J. F. Nye and M. V. Berry, "Dislocations in wave trains," *Proc. R. Soc. London Ser. A* **336**, 165–190 (1974).
- N. B. Baranova, B. Ya. Zel'dovich, A. V. Mamaev, N. F. Pilipetski, and V. V. Shkunov, "Speckle-inhomogeneous field wavefront dislocation," *Pis'ma Zh. Eks. Teor. Fiz.* **33**, 206–210 (1981) [*JETP Lett.* **33**, 195–199 (1981)].
- J. F. Nye, "Optical caustics in the near field from liquid drops," *Proc. R. Soc. London Ser. A* **361**, 21–41 (1978).
- A. M. Deykoon, M. S. Soskin, and G. A. Swartzlander, Jr., "Nonlinear optical catastrophe from a smooth initial beam," *Opt. Lett.* **24**, 1224–1226 (1999).
- G. A. Swartzlander, Jr. and C. T. Law, "Optical vortex solitons observed in Kerr nonlinear media," *Phys. Rev. Lett.* **69**, 2503–2506 (1992).
- A. W. Snyder, L. Poladian, and D. J. Michell, "Parallel spatial solitons," *Opt. Lett.* **17**, 789–791 (1992).
- G. A. Swartzlander, Jr., "Peering into darkness with a vortex spatial filter," *Opt. Lett.* **26**, 497–499 (2001).
- D. Palacios, D. Rozas, and G. A. Swartzlander, "Observed scattering into a dark optical vortex core," *Phys. Rev. Lett.* **88**, 103902 (2002).
- D. Rozas, Z. S. Sacks, and G. A. Swartzlander, Jr., "Experimental observation of fluid-like motion of optical vortices," *Phys. Rev. Lett.* **79**, 3399–3402 (1997).
- L. Allen, M. W. Beijersbergen, R. J. C. Spreeuw, and J. P. Woerdman, "Orbital angular momentum of light and the transformation of Laguerre–Gaussian laser modes," *Phys. Rev. A* **45**, 8185–8189 (1992).
- I. V. Basistiy, V. Y. Bazhenov, M. S. Soskin, and M. V. Vasnetsov, "Optics of light beams with screw dislocations," *Opt. Commun.* **103**, 422–428 (1993).
- V. Y. Bazhenov, M. V. Vasnetsov, and M. S. Soskin, "Laser beams with screw dislocations in their wavefronts," *Pis'ma Zh. Eks. Teor. Fiz.* **52**, 1037–1039 (1990) [*JETP Lett.* **52**, 429–431 (1990)].
- V. Y. Bazhenov, M. S. Soskin, and M. V. Vasnetsov, "Screw dislocations in light wavefronts," *J. Mod. Opt.* **39**, 985–990 (1992).
- V. P. Lukin and V. V. Pokasov, "Optical wave phase fluctuations," *Appl. Opt.* **20**, 121–135 (1981).
- P. Couillet, L. Gill, and F. Rocca, "Optical vortices," *Opt. Commun.* **73**, 403–408 (1989).
- C. T. Law and G. A. Swartzlander, Jr., "Optical vortex solitons and the stability of dark soliton stripes," *Opt. Lett.* **18**, 586–588 (1993).
- K. Staliunas, "Dynamics of optical vortices in a laser beam," *Opt. Commun.* **90**, 123–127 (1992).
- G. Indebetouw, "Optical vortices and their propagation," *J. Mod. Opt.* **40**, 73–87 (1993).
- I. Freund, "Optical vortex trajectories," *Opt. Commun.* **181**, 19–33 (2000).
- I. Velchev, A. Dreischuh, D. Neshev, and S. Dinev, "Interaction of optical vortex solitons superimposed on different background beams," *Opt. Commun.* **130**, 385–392 (1996).
- L. V. Kreminskaya, M. S. Soskin, and A. I. Krizhnyak, "The Gaussian lenses give birth to optical vortices in laser beams," *Opt. Commun.* **145**, 377–384 (1998).
- D. Rozas, C. T. Law, and G. A. Swartzlander, "Propagation dynamics of optical vortices," *J. Opt. Soc. Am. B* **14**, 3054–3065 (1997).
- F. S. Roux, "Dynamical behavior of optical vortices," *J. Opt. Soc. Am. B* **12**, 1215–1221 (1995).
- D. Rozas, Z. S. Sacks, and G. A. Swartzlander, "Experimental observation of fluid-like motion of optical vortices," *Phys. Rev. Lett.* **79**, 3399–3402 (1997).
- L. C. Crasovan, G. Molina-Terriza, J. P. Torres, L. Torner, V. M. Perez-Garcia, and D. Mihalache, "Globally linked vortex clusters in trapped wave fields," *Phys. Rev. E* **66**, 036612 (2002).
- C. T. Law and G. A. Swartzlander, Jr., "Polarized optical vortex solitons: instabilities and dynamics in Kerr nonlinear media," *Chaos, Solitons Fractals* **4**, 1759–1766 (1994).
- H. J. Lugt, *Vortex Flow in Nature and Technology* (Wiley-Interscience, New York, 1983).